Comparison of Various Modelling Techniques to Estimate Land Surface Temperature: A Case Study from Prince Edward Island, Canada

Usman Ali[1], Travis Esau[1], Aitazaz A. Farooque[2*], Farhat Abbas[2], Bilal Ahmad[3]

Abstract— Land surface temperature (LST) is a key factor in climate change studies. It is largely affected and thus predicted by the land uses in urban areas. The presented study identified the explanatory power of urban index (UI), modified soil adjusted vegetation index (MSAVI), modified normalized water index (MNDWI), elevation, aspect, and hill shade to predict the LST using the ordinary least square regression, spatial lag, spatial error and geographically weighted models. The UI has shown a direct relationship with LST, and the rest of the explanatory variables have shown an indirect relationship with LST. The Akaike info criterion (AIC) values were used as a standard for comparison of the regression models. The ordinary least square (OLS) regression model has achieved the highest AIC value of 886 and the lowest R^2 (0.73). The spatial lag model (SLM) and spatial error model (SEM) achieved the AIC value respectively, 715 and 681. The SLM and SEM achieved the R^2 of 0.85 and 0.89, respectively, which are considerably higher than that of the OLS model. The geographical weight regression (GWR) achieved the lowest AIC value, 669, and the highest R^2 (0.93). The study proved that the GWR model can be used for predicting LST compared to OLS, SLM, and SEM models. This finding will help the urban planner select a suitable regression model for predicting the LST and an effective way to predict the LST for understanding the effects of climate change through modeling LST.

Index Terms— Landsat-8, Land surface temperature, Vegetation indices, Ordinary least square regression model, Spatial lag model, Spatial error model

IJSER

1 Introduction

The growth of world urbanization has increased after the second world war. This excessive growth has caused many undesired side effects on the environment. In Canadian regions, a 1.5 °C increase in the mean temperature has been observed from 1950 to 2010 [1]. Prince Edward Island (PEI) is a Canadian province and faces sectional warming, hotter days and nights resulting in increasing temperature [2]. This change in land surface temperature (LST) has been linked with global warming and will continue to affect agriculture, the ecological system, and environmental conditions [3]. This shows the importance and needs to find significant predictors and models to facilitate LST's prediction.

The LST rises as the percentage of paved surfaces increases in an area, as a paved surface stores heat during the day and slowly releases the heat during the evening [4]. Artificial heat released by commercial areas, vehicles, industrial activities, and domestic and industrial air conditioning increases the LST and atmospheric temperature within a city, and these factors are directly linked with urbanization [5]. Extensive urbanization is a major problem in the 21st century as it changes the land cover pattern and drastically affects the LST of any city [6]. Land use and land cover (LULC) of an area can estimate the LST as LST varies based on the land used pattern [7].

Many researchers have used a variety of algorithms and techniques to estimate the LST [8]. Remote sensing helps the researchers effectively estimate the LST due to the ample range availability of satellites like Landsat-7, Landsat-8, and Moderate Resolution Imaging Spectroradiometer (MODIS) [9].

Several studies have established the relationship between LST and satellite-based indices [10]. The abundant remote sensing indices have been industrialized, for example vegetation indexes (i.e., perpendicular vegetation index (PVI) [11], soil adjusted vegetation index (SAVI) [12], normalized difference vegetation index (NDVI) [13], band difference (DVI), atmospherically resistant vegetation index (ARVI) [14], modified normalized water index (MNDWI) [15], normalized built-up index (NDBI) [16], normalized difference bare land index (NDBaI), normalized bare land index (NBLI), and urban index (UI) [17] have been developed to establish a correlation with LST. The UI, MNDWI, and modified soil adjuted vegetion index (MSAVI) have greater potential to delineate the urban, water, and greenery. Beyond the change in the land cover pat-

- *Usman Ali[1] is a graduate student at the Faculty of Agriculture, Dalhousie University, Canada, PH- +19029166570. E-mail: usman.ali@dal.ca*
- *Travis Esau[1] is an Associate Professor in the Department of Engineering, Dalhousie University, Canada, PH- +19028933055. E-mail: tesau@dal.ca*
- *Aitazaz A. Farooque[2] is an Associate Professor in the Faculty of Sustainable Design Engineering and School of Climate Change and Adaptation, University of Prince Edward Island, Canada, PH- +19025666084. E-mail: afarooque@upei.ca*
- *Farhat Abbas[2] is a Research Associate at the School of Climate Change and Adaptation, University of Prince Edward Island, Canada, PH- +16479064510. E-mail: fabbas@upei.ca*
- *Bilal Ahmad[3] is a graduate student at the Faculty of Agricultural Engineering and Technology, University of Agriculture, Faisalabad, Pakistan, PH- +923064613921. E-mail: eabilal@yahoo.com*

*Correspondence: afarooque@upei.ca

tern effect on LST, it is observed that air temperature reduces with an increase in altitude; this reduction is called the lapse rate. Therefore, aspect, hill shade, and elevation can significantly increase or decrease the LST.

Land use is a spatially varying human-induced process that substantially affects the natural environment where spatial heterogeneity yields different results [18]. As a result, it is essential to incorporate spatial heterogeneity into the LST modelling to achieve better prediction for support of planning and decision making [19]. Few studies incorporate the spatial heterogeneity, spatial dependence, and autocorrelation problem in LST modelling [20]. This study compares the ordinary least square regression (OLS), spatial lag model (SLM), spatial error model (SEM), and geographically weighted regression (GWR) models and discusses the opportunities and limitations of each model.

The observed increase in PEI temperature emphasizes determining the spatial relationship between remote sensing indices that map out the land cover pattern and predict the LST. The adopted methodology is useful to quantify the extent of different predictors in the prediction of LST. The importance of this study is that it will help the local government with urban planning, as well as mitigate the risk of LST on the environment. Therefore, the specific objectives of this study include:

1. Identifying the significant predictors and their extent to predict the LST using a 10-ha tessellation scheme.
2. Identification of best fit model for predict the LST.

1.1 Study Area

This study was conducted in Summerside, Prince Edward Island, Canada (Figure 1). Summerside is the second-largest city in Prince Edward Island, Canada, and construction in this city increased by 40% when comparing 2019 to 2018. This city faces extensive urbanization; thus, the land cover pattern changes here and directly affect the LST. Prince Edward Island is a humid island, strongly influenced by the prevailing weather of its surroundings throughout the year. During the winter season, the island receives blizzards and storms originating from the Gulf of Mexico and North America. After 2013, changes in the Summerside land cover pattern were observed as it undergoes multiple construction projects [21]. For that reason, this city was selected for LST modelling.

2 Material and Methods

2.1 Data Sources

This study used Landsat-8 OLI-TIRS (2020) satellite images to prepare the UI, MSAVI, and MNDWI. The Landsat-8 OLI/TIRS thermal band (11) was used to calculate the surface temperature. The digital elevation model data was used to calculate the aspect and hill shade. Details regarding the data and methodology are represented in Table 1 and Figure 2.

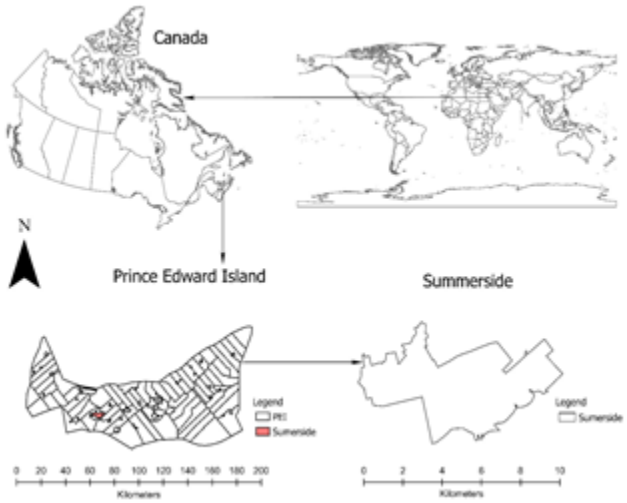

Figure 1: Summerside map placed along with Global Canadian and Prince Edward Island map.

Table 1: Landsat-8 OLI/TIRS data for calculating the vegetation indices and LST estimation.

Satellite Name	Path No. / Row No.	Cloud (%)
Landsat-8	007/028	1.34
	008/028	2.34
	008/027	0.03

2.2 Method to Estimate the Vegetation Indices to Delineate the Typical LULC Classes

Numerous indices have been published to establish the relationship with LST. Based on the literature review, this study selected the most efficient indices representing water, greenery, and urban areas (Table 2). The formulas mentioned in Table 2 were used to calculate these indices. The study area is divided into 10-ha hexagonal grids to calculate the mean value of each index in these grids (Figure 3). All these processing steps were done by using ArcGIS Pro geoprocessing tools.

Table 2: Vegetation indices related to typical LULC Types.

Types	Index	Formula	Reference
Vegetation Index	MSAVI	$((2NIR+1)\sqrt{(2NIR+1)^2-8(NIR+Red)})/8$	[1]
Water Index	MNDWI	(Green-SWIR)/(Green+SWIR)	[30]
Built-up index	UI	(SWIR2-NIR)/(SWIR2+NIR)	[12]

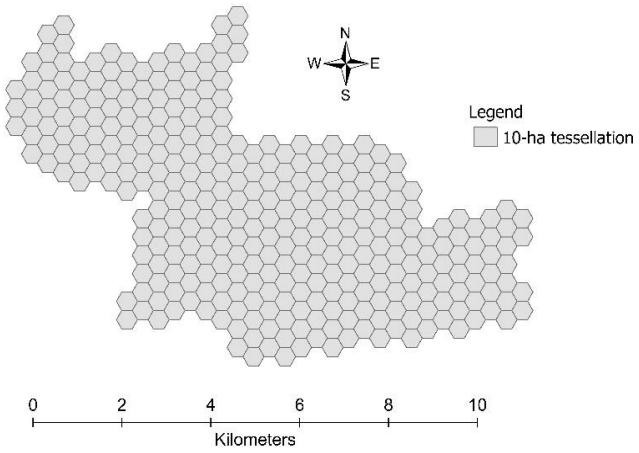

Figure 2: Summerside area divided into 10-ha tessellation for extracting the mean values of dependent and independent variables in each tessellation corresponding to its GRID ID.

2.3 Method for Retrieving the LST from the Thermal Band of Landsat-8

The satellite images first underwent the preprocessing stages, namely, mosaicking and clipping. Following this, the clipped study areas were used for LST estimation. For calculating the LST, only band 11, band 5, and band 4 were used. Landsat-8 OLI/TIRS band 11 is a thermal infrared band, band 5 is the inferred band, and band 4 is red. The spectral radiance method was used to estimate the LST from Landsat-8 OLI/TIRS [22]. Digital number (DN) was converted into radiance with the help of equation 1.

$$L = ML \times Q_{CAL} + AL \quad (1)$$

Here, L represents the spectral radiance, ML is the band-specific multiplicative rescaling factor, AL is the band-specific additive rescaling factor, and Q_{CAL} is a thermal band.

After extracting the radiance, it was converted into the top atmosphere brightness temperature using the following equation.

$$TB = ((K2/\ln((K1/L)+1))-273 \quad (2)$$

Here, the atmosphere surface temperature is TB, K1, and K2 are thermal conversions constant. To convert the surface temperature units from Kelvin to Celsius, absolute zero (-273.5) was added to the equation 2 [23].

To calculate the LST using Landsat-8 OLI/TIRS, values from equations 1 and 2, vegetation fiction (F_v), and emissivity were used [24].

$$F_v = ((NDVI-NDVImin)/(NDVImax-NDVImin))^2 \quad (3)$$

$NDVI_{min}$ value represents the bare soil, and $NDVI_{max}$ value, indicating healthy vegetation [25].

Emissivity was calculate using the following formula.

$$\varepsilon = 0.004 \times Fv + 0.986 \quad (4)$$

Finally, LST was calculated using the following equations [9].

$$LST = ((TB)/(1+((\lambda \times TB)/hc)\ln(\varepsilon)) \quad (5)$$

Here, h is Planks constant (6.626 × 10-34 Js), c is the velocity of light (2.98 × 10-8m/s), λ is the effective wavelength (12.00 for band 11 in Landsat-8), σ is the Boltzman constant (1.38 × 10-23 J/K). The calculated LST range varies from 14 to 26 °C represented in Figure 3. The mean values of LST in 10-ha hexagonal grids were calculated using the zonal statistic tool as shown in Figure 2 to establish the relationship with explanatory variables.

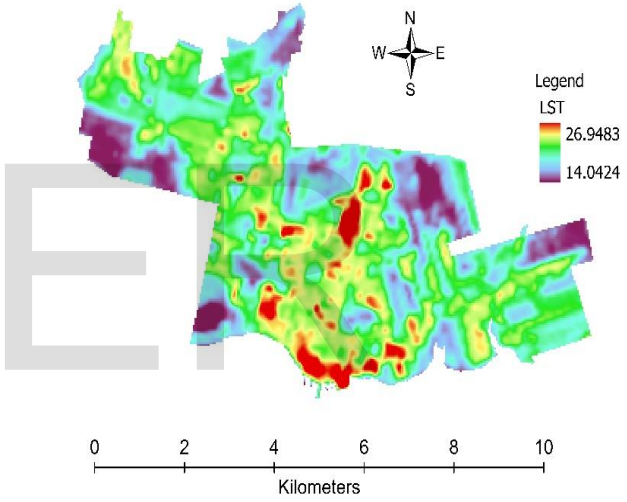

Figure 3: Land surface temperature of Summerside study area calculated based on Landsat-8 data, variation visualization.

2.4 Elevation, Aspect, Hill Shade, UI, MNDVI and MSAVI

A hill shade is a grayscale 3D representation of the surface, with the sun's relative position considered for shading the image. Elevation data mentioned above was used to calculate the aspect and hill shade using ArcGIS Pro geoprocessing tools. The Azimuth and altitude in the hill shade tool were set as respectively 315 and 45°. The vegetation indices UI, MNDWI, and MSAVI were calculated using equations mentioned in Table 2 with the help of the geoprocessing tool of Arc GIS Pro. The study area was divided into several 10-ha hexagonal tessellations and the elevation, aspect, hill shade, UI, MNDWI, MSAVI, and LST mean values in each hexagonal grid were calculated using zonal statistics as a table tool available in ArcGIS Pro. The OLS, SLM, SEM, and GWR model accuracy compared for predicting the LST.

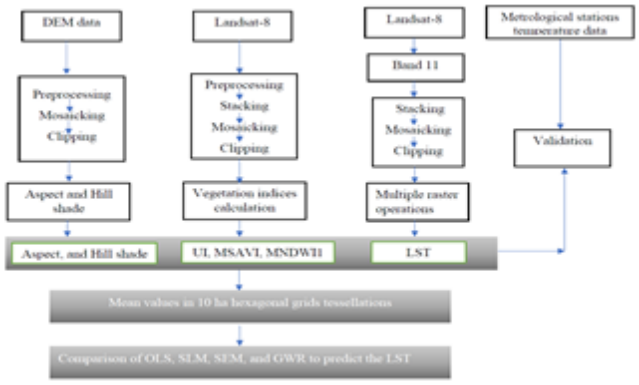

Figure 4. The flow diagram explaining the methodology of this study.

2.5 Ordinary Least Square Model, Spatial Lag Model, Spatial Error Model and Geographically Weighted Model

ArcGIS Pro and GeoDa software is most suitable for spatial analysis. The regression models OLS, SLM, SEM, and GWR were compared and tried to verify assumptions. The OLS first applied, and based on the OLS diagnostic output, verified the assumptions. The bivariate Moran's I test was applied to check the spatial structure of data and the explanatory power of each independent variable to predict the LST. The relationship between variables, namely, surface temperature vs. MSAVI, U1, MNDWI, elevation, aspect, and hill shade, has been verified using bivariate Moran's I scatter plot. Global Moran's I test output verified spatial autocorrelation between the residuals. Homoscedasticity and multicollinearity between the variables have been verified by interpreting the Koenker-Bassett and Jarque-Bra test. The OLS regression violated the assumption, as the Lagrange multiplier (lag) and Lagrange multiplier (error) were significant in OLS spatial dependence output. Therefore, spatial lag and spatial error models were run. The heteroskedasticity problem was observed in both models because these models do not account for the non-stationarity process. The GWR was applied, as it can take into account the non-stationary process. In the end, the model performance was assessed based on statistical criteria Akaike's information criterion (AIC) proposed by [26]. The higher the AIC value, the weak model fit [27]. The accuracy of model fitting was evaluated based on the root mean square error.

3 Results

3.1 Distribution of Estimated LST and Compared With Air Temperature

Generally, the remote sensing-based calculated LST was compared with air temperature acquired from metrological stations for validation [28]. Following the same method, we compared the calculated LST with air temperature acquired from metrological stations. The difference between estimated LST and air temperature is minimal; with potential reasons behind this being win speed, surface type, time of observation, and drastically decreasing air temperature [29]. The comparison between calculated LST and air temperature for Summerside is represented in Figure 5. The blue colour in the maps represents the lowest LST, and the red colour represents the highest LST.

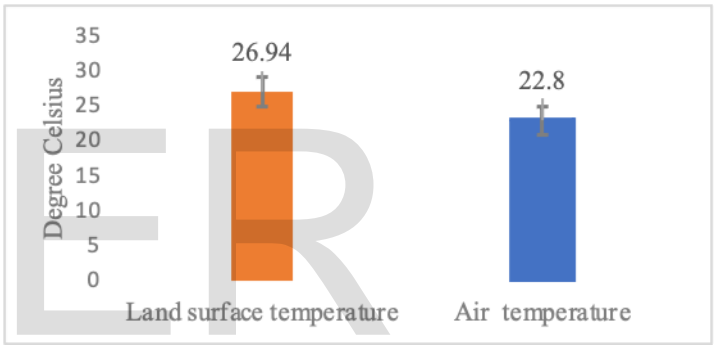

Figure 5: Land Surface Temperature and Air Temperature Difference in Summerside (°C).

3.2 Predictors of LST

In this study, UI, MNDWI, MSAVI, aspect, hill shade, and elevation have been used as predictors of LST (Figure 6). Figure 6 shows that where the high value of MSAVI is experienced, LST decreases. Similarly, where the high value of UI was experienced, LST increased because nearby buildings absorb the radiations (Figure 6). Also experienced that LST decreases as we moved from low elevation to high elevation areas (Figure 6). These findings are also supported by recent publications [30].

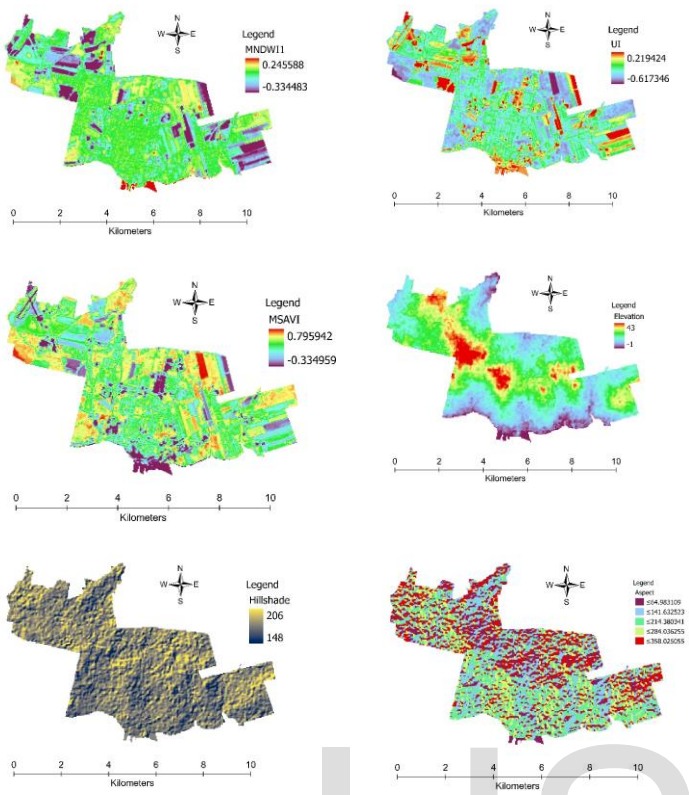

Figure 6: Pattern change visualization of MNDWI1, MSAVI, UI, elevation, aspect and hill shade in Summerside, PEI.

3.3 Predictors Explanatory Power

All explanatory variables were used in regression, and one explanatory variable was added at a time for estimating the explanatory power of each variable. MSAVI, UI, MNDWI, and elevation had good explanatory power to predict the LST. Bivariate Moran's I test identified that the MSAVI has a negative relationship (Moran's I = -0.43) with LST (Figure 4). MNDWI has a negative relationship (Moran's I = -0.041) with LST. Figure 4 also showed that UI has a strong positive relationship, and elevation showed a week relationship with LST. Moran's, I showed that aspect, and hill shade negatively relates to LST but has low explanatory power (Figure 7).

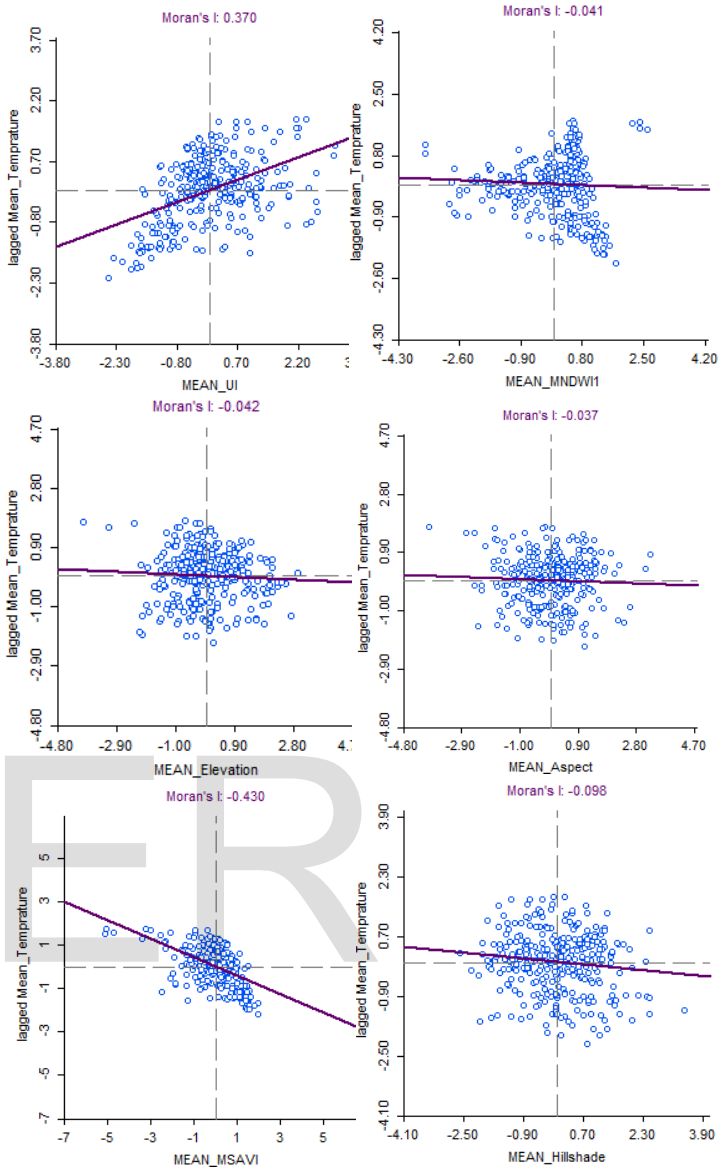

Figure 7: Bivariate Moran's I result identified the relationship and explanatory power of MNDWI1, UI, MSAVI, elevation, aspect and hill shade with LST.

3.4 Comparison of Ordinary Least Model, Spatial Error Model, Spatial Lag Model and Geographically Weighted Model

A first ordinary least regression model was brought into service to predict significant variables for measuring the LST. MNDWI, U1, MSAVI, aspect, elevation, and hill shade were explanatory variables for predicting the LST in Summerside. The R^2 = 0.73 was achieved. The output of diagnostic OLS proved that the OLS model violated the assumptions. In the Multicollinearity condition, number > 20 multicollinearities are concerned. Jarque-Bra output P < 0.05 represents that lack of normality. Koenker-Bassett test P < 0.05 indicates it has heteroskedasticity. Moran's I DF = 0.539 represents it has spatial dependence in the residuals. Lagrange Multiplier (lag) and

IJSER

Lagrange multiplier (error) P > 0.05 allowed to run the SLM and SEM. The OLS model AIC value is 886, which was bigger than other models (Figure 8).

The overall fit of the SLM was strong (R^2 = 0.85), which was considerably higher than the OLS model. Breusch-Pagan test and likelihood ratio test P < 0.05 indicated that this model also has heteroskedasticity and the spatial dependent issue still exists (Table 3).

Table 3: Breusch-Pagan Test and Likelihood Ratio Test for validation of assumption.

Model	Breusch-Pagan Test	Likelihood Ratio Test
OLS	0.0000	0.0000
SLM	0.0001	0.0000
SEM	0.0000	0.0000
GWR	-	-

The SLM only counted the stationary process, and this process is non-stationary. The AIC value is 715 less than the OLS model AIC; this indicated that the spatial lag model has good compared to the OLS model (Figure 8).

The overall fit of the SEM was stronger (R^2 = 0.89) than compared to OLS and SLM. Breusch-Pagan test and likelihood ratio test P < 0.05 in this model show heteroskedasticity and the spatial dependent issue is still present in this model (Table 3). Interestingly, the SEM yielded 681 AIC, which is less than the OLS and SLM AIC values (Figure 8).

This process is non-stationary as the above-mentioned predictor variables will not show the same relationship with LST at any other study area. The OLS, SLM, and SEM consider the stationary process. The GWR is best to account for the non-stationarity process. The GWR model yielded the R^2 = 0.93 which is stronger than other regression models. This model has corrective action for spatial varying parameters. That's why the non-stationarity problem in the above models is accounted to replace with the GWR model. The AIC value of GWR was 669 and this lowest AIC value and highest R^2 than other models proved that the GWR regression model is suitable to predict the LST (Figure 8).

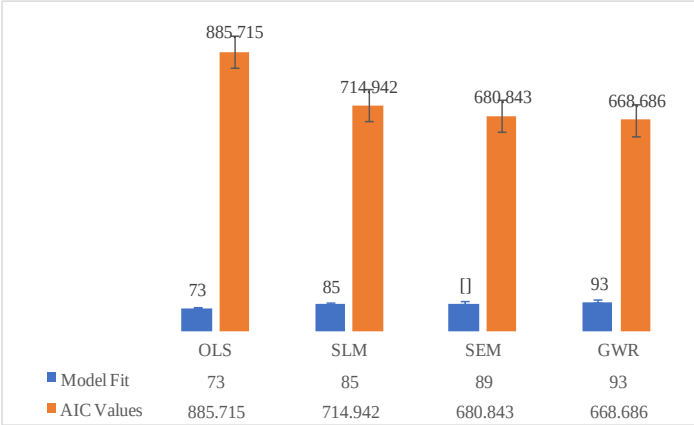

Figure 8: AIC value-based comparison of OLC, SLM, SEM and GWR models for LST modelling.

4 DISCUSSION

This study clarifies the extant explanatory variables in 10-ha hexagonal grids to predict the LST. The UI showed a positive relationship with LST. However, this analysis resulted in a negative relationship between MSAVI, MNDWI with LST. The evaluation, hill shade, and aspect showed a weak negative relationship with LST, and these results were also supported by published research [31]. Normally, random control points are used in the study area to predict the LST. The random points are not able to account for explanatory, and dependent variables' values variability for a whole study area. Furthermore, few studies incorporated the assumption of regression models to avoid bias in the model prediction [32]. This analysis divided the whole study area into the 10 ha hexagonal grids tessellation, calculated the mean value of each explanatory variable and LST, and verified the assumptions of spatial regression models. Due to this method, higher R^2 was achieved by each model as compared to a recent publication [34].

Machine Learning approaches are applied to predict the LST using multiple explanatory variables, but these have limitations in addressing spatial data's heterogeneity, stationarity, and non-stationary assumption [16]. Ignoring these assumptions causes significant misleading in model predictions. The model performance depends on their characteristics and natures. Spatial regression models SLM, SEM, and GWR models are designed to improve the model fit than the traditional OLS model by incorporating the spatial autocorrelation, stationarity, and non-stationary process [34]. The diagnostic table of OLS revealed that a significant positive autocorrelation exists between explanatory variables and LST and showed that SLM, SEM are both significant. Therefore, the OLS model was not valid to predict the LST. The SLM and SEM increased the modelling accuracy, but the Breusch-pagan test and likelihood

ratio test significant (Table 4) proved that the heteroskedasticity problem still exists. The accuracy of these models is higher as compared to the OLS model but less than the GWR model. The potential reason for this was that both SLM and the SEM model do not account for the non-stationarity process. These models only accounted for the spatial dependence in residuals and variables, and the GWR model can account for the non-stationarity process [34]. This analysis is a non-stationarity process; for example, all the above-mentioned explanatory variables used to predict the LST in this region will not show the same relationship with LST in other regions. GWR is a local spatial model which uses a moving window over a spatially distributed set of observations and produces a set of model coefficients from subsamples of data around the specific points in space. The GWR accounted for the spatial autocorrelation and non-stationarity process [34]. Therefore, the GWR model fitted the data better and produced more desirable results.

The four models namely, OLS, SLM, SEM, and GWR compared based on the AIC presented in Figure 5. The AIC values have an inverse relationship with model accuracy [27]. In this analysis, the OLS model has the highest AIC value compared to the SLM, SEM, and GWR model, and model fit is less than other models (Figure 5). The SLM and SEM also have higher AIC values than the GWR model, and the model fits less than GWR. The lowest AIC value yielded by GWR and proved the highest model fit.

5 Conclusions

This study demonstrates that Landsat-8 OLI/TIRS images are useful for assessing the LST, MSAVI, UI, MNDWI, and ASTER DEM data to estimate the elevation hill shade and aspect. The high LST recorded showed higher UI, lower MSAVI, lower elevation, and lower hill shade values. The present study used the six explanatory variables (UI, MSAVI, MNDWI, elevation, aspect, hill shade) to predict the LST. These all-explanatory variables explained the maximum 93% LST using the GWR model and achieved the lowest AIC value 669. This model also concludes that an increase in built-up land is a serious threat that increases the LST. Vegetation and hill shade play an important role in mitigating the increase in LST. Because of this, suitable ways to decrease the built-up area are not available, and the only viable option is to increase the green spaces to mitigate the risk of increasing the LST.

The regression models are very useful to predict the LST. Thus, some models can incorporate heteroskedasticity and non-stationarity assumptions. Therefore, this study used OLS, SLM, SEM, and GWR models to determine the best fit model to predict the LST. The OLS model was first applied, and heteroskedasticity and spatial dependence problems were present in the residuals. The OLS model cannot account for these problems. The SLM and SEM models can account for the spatial dependence, but unfortunately, they do not handle the heteroskedasticity problem because they assume each process stationarity. In contrast, the GWR models incorporate spatial dependence and heteroskedasticity into the modelling process consequently, fit the data better and predict the response variable accurately. GWR is also a useful model for handling the non-stationarity at different spatial scales. This study results also proved that the GWR model is appropriate for predicting the LST. The findings of this study help the specific government of PEI to mitigate the risk of LST in main cities, and contrast also helps select the regression model for predicting the LST using multiple variables.

References

[1] Vincent, L. A., Wang, X. L., Milewska, E. J., Wan, H., Yang, F., & Swail, V. (2012). A second generation of homogenized Canadian monthly surface air temperature for climate trend analysis. *Journal of Geophysical Research Atmospheres*, *117*(17), 1–13. https://doi.org/10.1029/2012JD017859

[2] Maqsood, J., Farooque, A. A., Wang, X., Abbas, F., Acharya, B., & Afzaal, H. (2020). Contribution of climate extremes to variation in potato tuber yield in Prince Edward Island. *Sustainability (Switzerland)*, *12*(12). https://doi.org/10.3390/SU12124937

[3] Mclachlan, J., Plant, A., & Garbary, D. J. (2018). *Demonstrating Climate Change in Prince Edward Island – A Procedure using Climate Normals and Weather*. *49*, 293–311.

[4] Kardinal Jusuf, S., Wong, N. H., Hagen, E., Anggoro, R., & Hong, Y. (2007). The influence of land use on the urban heat island in Singapore. *Habitat International*, *31*(2), 232–242. https://doi.org/10.1016/j.habitatint.2007.02.006

[5] Liu, L., & Zhang, Y. (2011). Urban heat island analysis using the landsat TM data and ASTER Data: A case study in Hong Kong. *Remote Sensing*, *3*(7), 1535–1552. https://doi.org/10.3390/rs3071535

[6] RIZWAN, A. M., DENNIS, L. Y. C., & LIU, C. (2008). A review on the generation, determination and mitigation of Urban Heat Island. *Journal of Environmental Sciences*, *20*(1), 120–128. https://doi.org/10.1016/S1001-0742(08)60019-4

[7] Weng, Q. (2003). Fractal Analysis of Satellite-Detected Urban Heat Island Effect. *Photogrammetric Engineering and Remote Sensing*, *69*(5), 555–566. https://doi.org/10.14358/PERS.69.5.555

[8] Bernales, A. M., Antolihao, J. A., Samonte, C., Campomanes, F., Rojas, R. J., Dela Serna, A. M., & Silapan, J. (2016). Modelling the relationship between land surface temperature and landscape patterns of land use land cover classification using multi linear regression models. *International Archives of the Photogrammetry, Remote Sensing and Spatial Information Sciences - ISPRS Archives*, *41*(January), 851–856. https://doi.org/10.5194/isprsarchives-XLI-B8-851-2016

[9] Avdan, U., & Jovanovska, G. (2016). Algorithm for automated mapping of land surface temperature using LANDSAT 8 satellite data. *Journal of Sensors*, *2016*. https://doi.org/10.1155/2016/1480307

[10] Kayet, N., Pathak, K., Chakrabarty, A., & Sahoo, S. (2016). Urban heat island explored by co-relationship between land surface temperature vs multiple vegetation indices. *Spatial Information Research*, *24*(5), 515–529. https://doi.org/10.1007/s41324-016-0049-3.

[11] Richardson, A. J., & Wiegand, C. L. (1977). Distinguishing

vegetation from soil background information. *Photogrammetric Engineering and Remote Sensing*, *43*(12), 1541–1552.

[12] A. R. Huete. (1988). A Soil-Adjusted Vegetation Index (SAVI). *Remote Sensing of Environment 25:295-309 (1988) A*, *25*, 295–309.

[13] Li, P., & Moon, W. M. (2004). Land cover classification using MODIS–ASTER airborne simulator (MASTER) data and NDVI: A case study of the Kochang area, Korea. *Canadian Journal of Remote Sensing*, *30*(2), 123–136. https://doi.org/10.5589/m03-061

[14] Kaufman, Y. J., & Tanré, D. (1992). Atmospherically Resistant Vegetation Index (ARVI) for EOS-MODIS. *IEEE Transactions on Geoscience and Remote Sensing*, *30*(2), 261–270. https://doi.org/10.1109/36.134076

[15] Xu, H. (2006). Modification of normalised difference water index (NDWI) to enhance open water features in remotely sensed imagery. *International Journal of Remote Sensing*, *27*(14), 3025–3033. https://doi.org/10.1080/01431160600589179

[16] Zha, Y., Gao, J., & Ni, S. (2003). Use of normalized difference built-up index in automatically mapping urban areas from TM imagery. *International Journal of Remote Sensing*, *24*(3), 583–594. https://doi.org/10.1080/01431160304987

[17] Kawamura, M.; Jayamana, S.; Tsujiko, Y. (2013). Relation between social and environmental conditions in Colombo Sri Lanka and the urban index estimated by satellite remote sensing data. *Journal of the American Medical Directors Association*, *14*(10), 731–735. https://doi.org/10.1016/j.jamda.2013.04.003

[18] Gao, C., Feng, Y., Tong, X., Lei, Z., Chen, S., & Zhai, S. (2020). Modeling urban growth using spatially heterogeneous cellular automata models: Comparison of spatial lag, spatial error and GWR. *Computers, Environment and Urban Systems*, *81*(November 2019),

[19] Song, J., Du, S., Feng, X., & Guo, L. (2014). The relationships between landscape compositions and land surface temperature: Quantifying their resolution sensitivity with spatial regression models. *Landscape and Urban Planning*, *123*, 145–157. https://doi.org/10.1016/j.landurbplan.2013.11.014

[20] Fornango, R. J. (2010). When space matters: Spatial dependence, diagnostics, and regression models. *Journal of Criminal Justice Education*, *21*(2), 117–135. https://doi.org/10.1080/10511251003693652

[21] Colin Maclean. (2019).Hundreds of new residential units currently under development in Summerside. Assess online.https://www.saltwire.com/prince-edward-island/news/hundreds-of-new-residential-units-currently-under-development-in-summerside-301302/

[22] Şahin, M., Yildiz, B. Y., Şenkal, O., & Peştemalci, V. (2012). Modelling and Remote Sensing of Land Surface Temperature in Turkey. *Journal of the Indian Society of Remote Sensing*, *40*(3), 399–409. https://doi.org/10.1007/s12524-011-0158-3

[23] Tran, D. X., Pla, F., Latorre-Carmona, P., Myint, S. W., Caetano, M., & Kieu, H. V. (2017). Characterizing the relationship between land use land cover change and land surface temperature. *ISPRS Journal of Photogrammetry and Remote Sensing*, *124*, 119–132. https://doi.org/10.1016/j.isprsjprs.2017.01.001

[24] Carlson, T. N., & Ripley, D. A. (1997). On the relation between NDVI, fractional vegetation cover, and leaf area index. *Remote Sensing of Environment*, *62*(3), 241–252. https://doi.org/10.1016/S0034-4257(97)00104-1

[25] Guha, S., Govil, H., Dey, A., & Gill, N. (2018). Analytical study of land surface temperature with NDVI and NDBI using Landsat 8 OLI and TIRS data in Florence and Naples city, Italy. *European Journal of Remote Sensing*, *51*(1), 667–678. https://doi.org/10.1080/22797254.2018.1474494

[26] Vancutsem, C., Ceccato, P., Dinku, T., & Connor, S. J. (2010). Evaluation of MODIS land surface temperature data to estimate air temperature in different ecosystems over Africa. *Remote Sensing of Environment*, *114*(2), 449–465. https://doi.org/10.1016/j.rse.2009.10.002

[27] Wang, Q., Ni, J., & Tenhunen, J. (2005). Application of a geographically-weighted regression analysis to estimate net primary production of Chinese forest ecosystems. *Global Ecology and Biogeography*, *14*(4), 379–393. https://doi.org/10.1111/j.1466-822X.2005.00153.x

[28] Srivastava, P. K., Majumdar, T. J., & Bhattacharya, A. K. (2009). Surface temperature estimation in Singhbhum Shear Zone of India using Landsat-7 ETM+ thermal infrared data. *Advances in Space Research*, *43*(10), 1563–1574. https://doi.org/10.1016/j.asr.2009.01.023

[29] Gallo, K., Hale, R., Tarpley, D., & Yu, Y. (2011). Evaluation of the relationship between air and land surface temperature under clear- and cloudy-sky conditions. *Journal of Applied Meteorology and Climatology*, *50*(3), 767–775. https://doi.org/10.1175/2010JAMC2460.1

[30] Zha, Y., Gao, J., & Ni, S. (2003). Use of normalized difference built-up index in automatically mapping urban areas from TM imagery. *International Journal of Remote Sensing*, *24*(3), 583–594. https://doi.org/10.1080/01431160304987

[31] Peng, *et al.* (2020) 'Correlation analysis of land surface temperature and topographic elements in Hangzhou, China', *Scientific Reports*, 10(1), 1–16. doi: 10.1038/s41598-020-67423-6

[32] Páez, A., & Scott, D. M. (2004). Spatial statistics for urban analysis: A review of techniques with examples. *GeoJournal*, *61*(1), 53–67. https://doi.org/10.1007/s10708-005-0877-5

[33] Mirbagheri, B., & Alimohammadi, A. (2017). Improving urban cellular automata performance by integrating global and geographically weighted logistic regression models. *Transactions in GIS*, *21*(6), 1280–1297. https://doi.org/10.1111/tgis.12278

[34] Zhang, L., Ma, Z., & Guo, L. (2009). An evaluation of spatial autocorrelation and heterogeneity in the residuals of six regression models. *Forest Science*, *55*(6), 533–548. https://doi.org/10.1093/forestscience/55.6.533

IJSER